Japanese Journal of Radiology (2019) 37:473–480
https://doi.org/10.1007/s11604-019-00829-z

ORIGINAL ARTICLE

T2*-weighted MR imaging findings of giant cell tumors of bone: radiological–pathological correlation

Hironori Nishibori[1] · Hiroki Kato[2] · Masaya Kawaguchi[2] · Akihito Nagano[3] · Masayuki Matsuo[2]

Received: 10 December 2018 / Accepted: 6 March 2019 / Published online: 11 March 2019

Abstract

Purpose To assess the correlation between T2*-weighted MR imaging and pathological findings of giant cell tumors (GCT) of bone.

Methods Of the 33 patients with histopathologically proven GCT of bone, 12 were examined using 1.5-T MR imaging, including T2*-weighted imaging, and were included in this study. The imaging and pathological findings of GCTs were compared between GCTs with and without hypointensity on T2*-weighted images (T2* hypointensity).

Results T2* hypointensity was observed in 6 out of 12 (50%) GCTs. Septal formation (83% vs. 17%; $p < 0.05$) and cystic formation (67% vs. 0%; $p < 0.05$) on T2-weighted images was significantly more frequent in the GCTs with T2* hypointensity compared with those without T2* hypointensity. Among the six GCTs with T2* hypointensity, a large amount of hemosiderin deposition was pathologically observed in five (83%) cases, whereas small amounts of hemosiderin deposition was seen in one (17%) case. In contrast, among the six GCTs without T2* hypointensity, a small amount of hemosiderin deposition was pathologically observed in all six (100%).

Conclusion Half of the GCTs showed T2* hypointensity, which is characteristic of hemosiderin deposition; whereas, the other half did not show T2* hypointensity due to a small amount of hemosiderin deposition.

Keywords Giant cell tumors of bone · MRI · T2*-weighted images · Hemosiderin

Introduction

Giant cell tumor (GCT) of bone is a benign but locally aggressive primary bone neoplasm that is composed of mononuclear cells, including numerous macrophages and large osteoclast-like giant cells. GCT represents approximately 5% of all primary bone tumors and 20% of benign bone tumors [1, 2]. Most GCTs affect skeletally mature patients, with slight female predominance. Although approximately 80% of cases occur between the ages of 20 and 50 years, GCTs can occur in the second decade of life or in individuals over 50 years of age [2, 3]. GCT arises in the metaphysis, with characteristic extension across a fused physis into the epiphysis, and typically affects the metaepiphyseal region of the long bone [4]. The most common site of GCT occurrence is the distal femur, followed by the proximal tibia, distal radius, sacrum, and proximal humerus [5, 6]. Atypical sites, including flat bone, small bones, and the spine are rarely involved.

Histologically, GCT is characterized by the presence of large multinucleated osteoclast-like giant cells, which are uniformly distributed throughout tumor, among numerous round or spindle-shaped mononuclear cells. GCT also contains numerous thin-walled vascular channels predisposing to areas of hemorrhage. Therefore, abundant hemosiderin deposition and hemorrhage are often observed within the tumor.

T2*-weighted gradient-echo imaging is a susceptibility-weighted sequence that is widely used for detecting hemorrhage, calcification, or hemosiderin deposition in various tissues and lesions. Unlike conventional spin-echo sequences, T2*-weighted imaging can detect microhemorrhages as small hypointense foci. This is due to its increased

✉ Hiroki Kato
hkato@gifu-u.ac.jp

[1] Department of Radiology, Kizawa Memorial Hospital, 590 Shimokobi, Kobi-cho, Minokamo City, Gifu 505-8503, Japan

[2] Department of Radiology, Gifu University School of Medicine, 1-1 Yanagido, Gifu 501-1194, Japan

[3] Department of Orthopedic Surgery, Gifu University School of Medicine, Gifu, Japan

sensitivity in detecting the presence of paramagnetic substances, which cause inhomogeneity in the magnetic field compared with conventional spin-echo sequences [7, 8]. Although blood products such as deoxyhemoglobin, methemoglobin, and hemosiderin are paramagnetic substances, T2*-weighted MR imaging is a sensitive method for hemosiderin detection owing to the strong paramagnetic effects of hemosiderin [9].

The solid components of GCTs often demonstrate low-to-intermediate signal intensity on T1- and T2-weighted images [2, 3, 5, 10, 11]. Although the cause of this signal intensity has been reported as hemosiderin deposition [10, 11], to the best of our knowledge, no previous reports have assessed the T2*-weighted imaging findings of GCTs. Therefore, this study aimed to assess the correlation between T2*-weighted MR imaging and pathological findings of GCT of bone.

Materials and methods

Patients

This study was approved by our institutional review board and complied with the guidelines of the Healthcare Insurance Portability and Accountability Act. Written informed consent was waived because this study was retrospective. The electronic medical chart system at Gifu University Hospital was queried for patients with histopathologically proven GCT of bone between November 2005 and April 2018. Among the 33 patients with histopathologically proven GCT of bone, 12 patients (mean age, 39 years; range, 19–60 years; seven men and five women) who underwent preoperative 1.5-T MR imaging, including T2*-weighted imaging, were included in this study (Table 1). The primary sites of GCT included the femur ($n=5$), tibia ($n=3$), radius ($n=2$), fibula ($n=1$), and cervical spine ($n=1$) (Table 2). All patients presented with local pain.

MR imaging

MR imaging was performed using 1.5-T MR imaging systems (Intera Achieva 1.5 T Pulsar, Philips Medical system, Best, The Netherlands or Signa Excite 1.5 T, GE Healthcare, Milwaukee, WI, USA). T2*-weighted gradient-echo (TR/TE 400–584/11–14 ms; flip angle 25–30°), T2-weighted fast spin-echo (TR/TE 4,000–4,200/94–106 ms), fat-suppressed T2-weighted fast spin-echo (TR/TE 2,815–4,000/86–106 ms), T1-weighted spin-echo (TR/TE 400–683/10–17 ms) images were obtained for all patients. T2*-weighted images were obtained in the transaxial plane ($n=7$), coronal plane ($n=3$), or sagittal plane ($n=2$). T2-, fat-suppressed T2-, and T1-weighted images were assessed using the same plane as T2*-weighted images. All MR images were obtained at a section thickness of 3–4 mm with a 1-mm intersection gap and a 12 × 12 – 35 × 35-cm field of view.

Image assessment

The MR images were retrospectively reviewed by two independent radiologists, who were unaware of the patients' clinical information, and who had 19–20 years of experience in post-training on musculoskeletal imaging. Any disagreement between the reviewers was resolved through consensus.

First, the reviewers assessed the presence of hypointensity within the tumors on T2*-weighted images (T2* hypointensity), suggestive of hemosiderin deposition. If T2* hypointensity was observed, the configurations of T2*

Table 1 The differences between giant cell tumors of the bone with and without T2* hypointensity

Hypointensity on T2*-weighted imaging	Present ($n=6$)	Absent ($n=6$)	p value
Male/female	4/2	3/3	0.500
Age (year)	31.0 ± 14.8	46.7 ± 10.6	0.065
Maximum diameter (mm)	62.5 ± 25.0	37.5 ± 7.2	0.065
T2-weighted imaging			
Hypointensity	6 (100)	4 (67)	0.227
Septal formation	5 (83)	1 (17)	0.040*
Cystic formation	4 (67)	0 (0)	0.030*
Fluid–fluid level formation	3 (50)	0 (0)	0.091
Internal homogeneity	0 (0)	2 (33)	0.227
T1-weighted imaging			
Hyperintensity	2 (33)	0 (0)	0.227

Note: data, excluding age and maximum diameter, are numbers of patients, and numbers in parentheses are frequencies expressed as percentages. Values of age and maximum diameter are the mean ± 1 standard deviation

*Significant difference was found between the two groups ($p<0.05$)

Table 2 The radiological and pathological findings of giant cell tumors of the bone

Patient no/age/sex	Location of the lesion	Radiological findings		Pathological findings	
		Hypointensity on T2*WI	Hypointensity on T2WI	Hemosiderin deposition	Hemorrhage
1/19/M	Left tibia	+	+	Large	Large
2/20/F	Left fibula	+	+	Large	Large
3/24/M	Right femur	+	+	Large	Large
4/32/F	Right femur	+	+	Large	Large
5/32/M	Left femur	+	+	Large	Large
6/59/M	Right femur	+	+	Small	Small
7/32/M	Left radius	−	+	Small	Large
8/53/F	Right tibia	−	+	Small	Large
9/54/F	Cervical spine	−	+	Small	Large
10/60/F	Right tibia	−	+	Small	Large
11/40/M	Left femur	−	−	Small	Small
12/41/M	Right radius	−	−	Small	Small

*T2*WI* T2*-weighted imaging, *T2WI* T2-weighted imaging, *large* large amount, *small* small amount

hypointensity were classified into two categories, including linear and nodular.

Second, the reviewers measured the maximum tumor diameter on T2-weighted images. T2-weighted images were also evaluated for the presence of well-circumscribed margins, endosteal scalloping, expansile growth, cortical disruption, hypointensity similar to skeletal muscles (T2 hypointensity), septal formation, cystic formation, fluid–fluid level formation, and internal homogeneity. Fat-suppressed T2-weighted images were assessed for the presence of periosteal reaction. T1-weighted images were assessed for the presence of hyperintensity in comparison to skeletal muscles (T1 hyperintensity).

Pathological assessment

A pathologist reviewed all open biopsy specimens. Pathological assessment of hemosiderin deposition and hemorrhage was performed using 10 consecutive medium power fields (200× magnification) stained with hematoxylin and eosin (H&E).

First, a pathologist classified the amount of hemosiderin deposition into two categories, including a large amount of hemosiderin deposition (observed in 5–10 fields) and a small amount of hemosiderin deposition (observed in 0–4 fields).

Second, a pathologist classified the amount of hemorrhage into two categories, including a large amount of hemorrhage (extravasated erythrocytes, which constituted more than half of areas, were observed in 5–10 fields) and a small amount of hemorrhage (extravasated erythrocytes, which constituted more than half of areas, were observed in 0–4 fields).

Statistical analysis

All statistical analyses were performed using SPSS version 22.0 (SPSS Inc, IBM, Chicago, IL, USA). The Mann–Whitney *U* test was used for comparing quantitative parameters, including patient age and maximum tumor diameter, between GCTs with and without T2* hypointensity. Chi-square test or Fisher's exact test was used for comparing the frequencies of T2 hypointensity, septal formation, cystic formation, fluid–fluid level formation, internal homogeneity on T2-weighted images, and T1 hyperintensity between GCTs with and without T2* hypointensity. A p value of less than 0.05 was considered to be statistically significant.

Results

T2* hypointensity was observed in 6 out of 12 (50%) GCTs (Figs. 1, 2). The configurations of T2* hypointensity were linear in 5 of 6 (83%) GCTs and nodular in 1 of 6 (17%) GCTs. On T2-weighted images, well-circumscribed margins and endosteal scalloping were observed in 12 of 12 (100%) GCTs, expansile growth in 11 of 12 (92%), cortical disruption in 10 of 12 (83%), T2 hypointensity in 10 of 12 (83%), septal formation in 6 of 12 (50%), cystic formation in 4 of 12 (33%), fluid–fluid level formation in 3 of 12 (25%), and internal homogeneity in 2 of 12 (17%). On fat-suppressed T2-weighted images, periosteal reaction was observed in 12 of 12 (100%) GCTs. T1 hyperintensity was observed in 2 of 12 (17%) GCTs.

Table 1 summarizes the differences between GCTs with and without T2* hypointensity. Marginally significant differences between GCTs with and without T2* hypointensity were observed for patient age (31.0 ± 14.8 years vs.

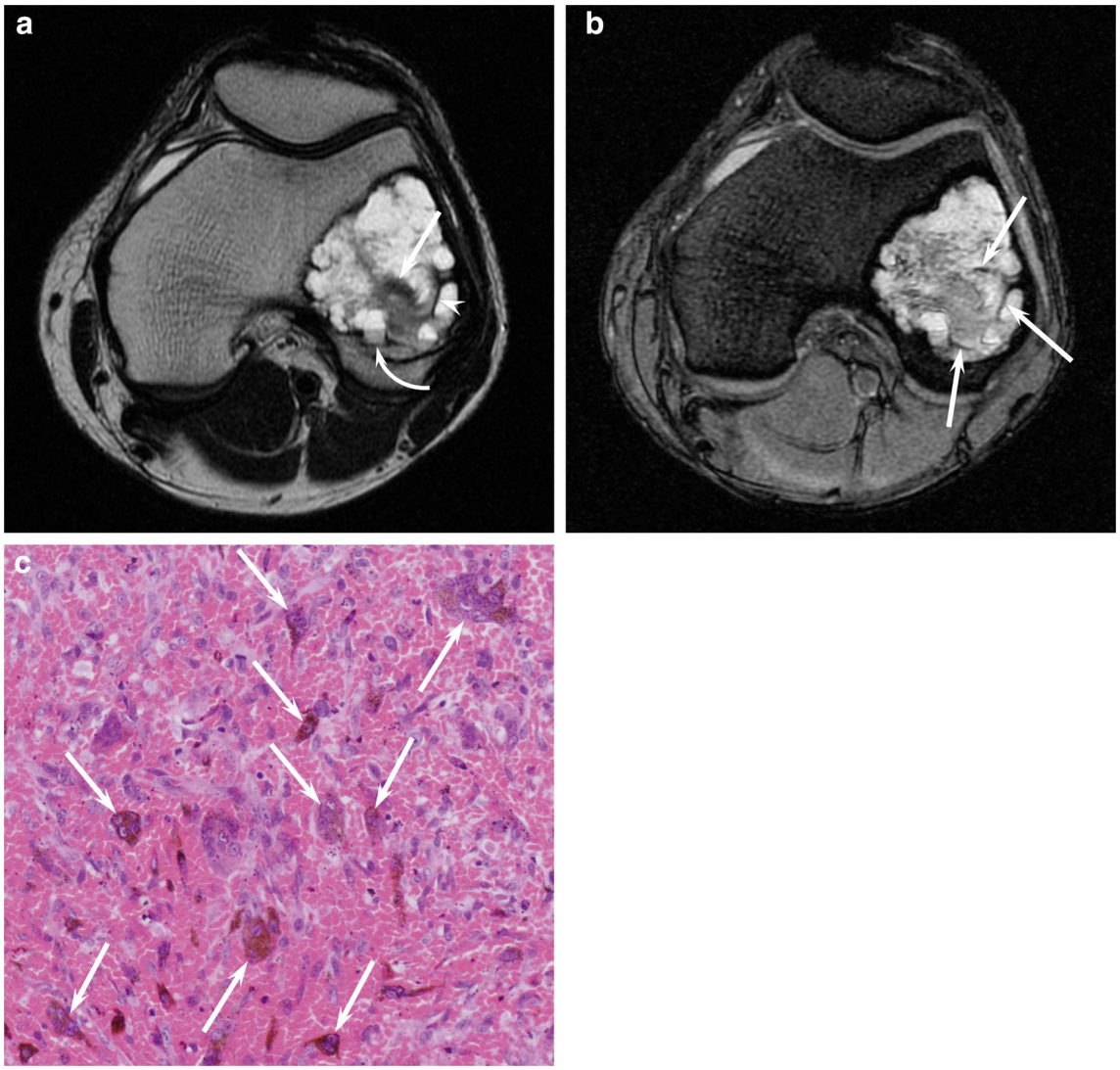

Fig. 1 A 32-year-old man with GCT of left distal femur (case 5). **a** T2-weighted fast spin-echo (TR/TE 4,000/106 ms) image shows a heterogeneous lesion with solid and cystic components. Hypointensity (arrow), septal formation (arrow head), cystic formation with fluid–fluid level (curved arrow) are demonstrated within the tumor. **b** T2*-weighted gradient-echo (TR/TE 584/13 ms) image shows linear hypointensies (arrows) within the tumor. **c** Open biopsy specimen (H&E stain, 200× magnification) shows hemosiderin deposition phagocytosed by macrophages (arrows) among numerous extravasated erythrocytes. This case was judged as a large amount of hemosiderin deposition and hemorrhage

46.7 ± 10.6 years, $p = 0.065$) and maximum tumor diameter (62.5 ± 25.0 mm vs. 37.5 ± 7.2 mm, $p = 0.065$). Septal formation (83% vs. 17%; $p < 0.05$) and cystic formation (67% vs. 0%; $p < 0.05$) on T2-weighted images was significantly more frequent in GCTs with T2* hypointensity compared to those without T2* hypointensity. However, no significant differences were noted between GCTs with and without T2* hypointensity in the frequency of T2 hypointensity (100% vs. 67%, $p = 0.227$), fluid–fluid level formation (50% vs. 0%, $p = 0.091$), internal homogeneity (0% vs. 33%, $p = 0.227$), and T1 hyperintensity (33% vs. 0%, $p = 0.227$).

The relationship between MR signal intensities and pathological findings is summarized in Table 2. A large amount of hemosiderin deposition was pathologically observed in 5 (cases 1–5) of 12 (42%) GCTs (Fig. 1) and a small amount of hemosiderin deposition was observed in 7 (cases 6–12) of 12 (58%) GCTs (Figs. 2, 3, 4). Among the six GCTs with T2* hypointensity, a large amount of hemosiderin deposition was pathologically observed in five (83%) cases (case 1–5) (Fig. 1), whereas a small amount of hemosiderin deposition was noted in one (17%) case (case 6) (Fig. 2). Conversely, among the six GCTs without T2* hypointensity, a small amount of hemosiderin deposition was pathologically observed in all six (100%)

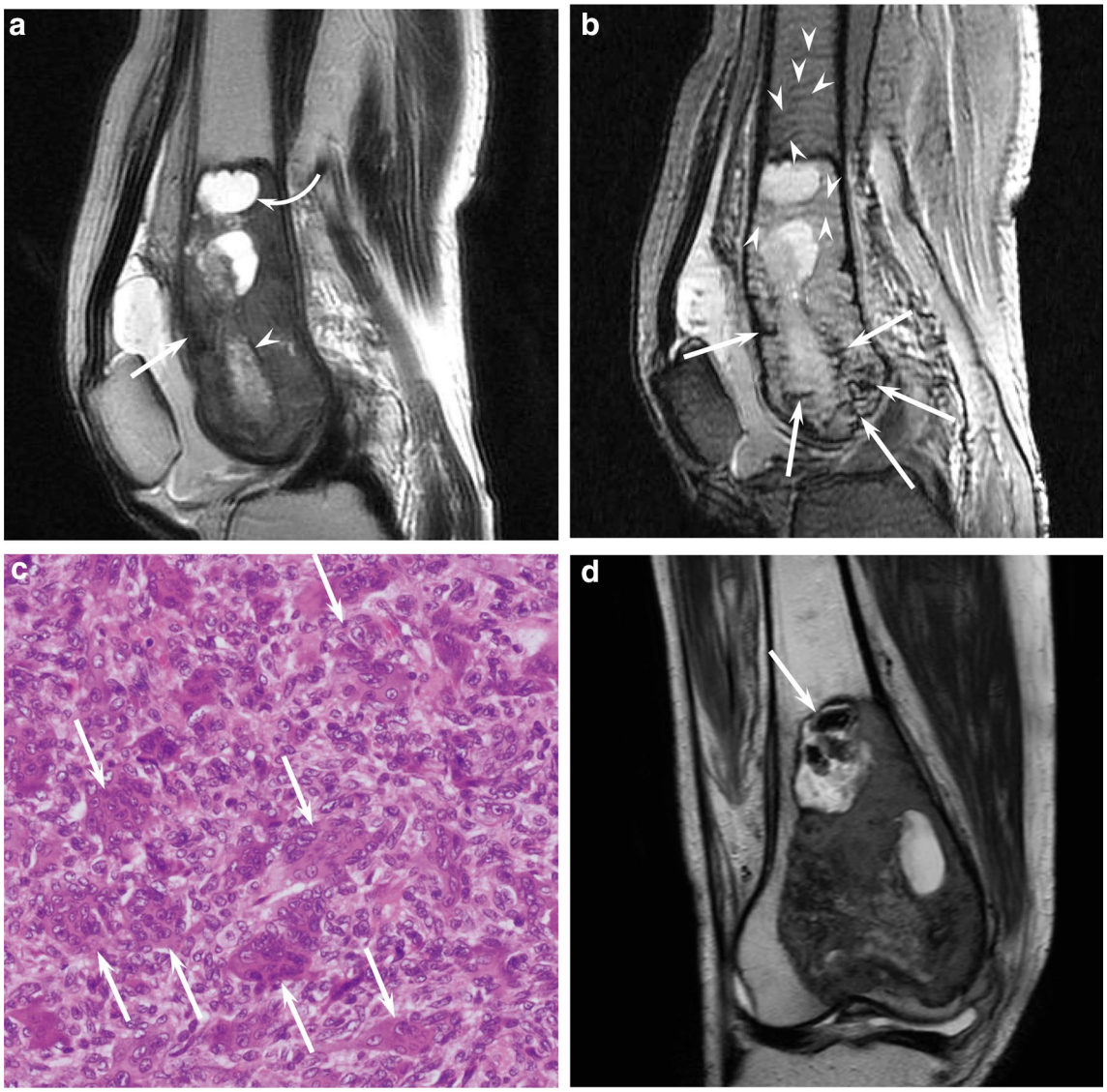

Fig. 2 A 59-year-old man with GCT of right distal femur (case 6). **a** T2-weighted fast spin-echo (TR/TE 4,000/100 ms) sagittal image shows a heterogeneous lesion with solid and cystic components. Hypointensity (arrow), septal formation (arrow head), cystic formation (curved arrow) are demonstrated within the tumor. **b** T2*-weighted gradient-echo (TR/TE 550/10 ms) sagittal image shows linear hypointensies distributed in middle or lower part of the tumor (arrows) and mildly hypointense stripes by truncation, Gibbs, or ringing artifacts (arrow heads). **c** Open biopsy specimen (H&E stain, 200× magnification) shows multinucleated giant cells without hemosiderin deposition (arrows). This case was judged as a small amount of hemosiderin deposition and hemorrhage. **d** T2-weighted fast spin-echo (TR/TE 4,000/100 ms) coronal image post open biopsy shows posttreatment change in upper part of the tumor (arrow)

(cases 7–12) (Figs. 3, 4). Meanwhile, a large amount of hemorrhage was pathologically observed in 9 (cases 1–5, 7–10) of 12 (75%) GCTs (Figs. 1, 3) and a small amount of hemorrhage was noted in 3 (cases 6, 11, 12) of 12 (25%) (Figs. 2, 4). Among the 10 GCTs with T2 hypointensity, a large amount of hemorrhage was pathologically observed in nine (90%) cases (cases 1–5, 7–10) (Figs. 1, 3), whereas a small amount of hemorrhage was observed in one (10%) case (case 6) (Fig. 2). Conversely, among the two GCTs without T2 hypointensity, a small amount of hemorrhage was pathologically observed in all two (100%) (cases 11–12) (Fig. 4). Thus, 2 out of 12 (17%) GCTs showed nonspecific hyperintensity without hypointense areas on T2*- and T2-weighted images, reflecting a small amount of hemosiderin deposition and hemorrhage (cases 11–12) (Figs. 4).

Discussion

On gross pathology, GCTs are eccentrically located in the metaepiphysis of long bones and extend to the articular surface. Usually, the overlying cortex undergoes resorption

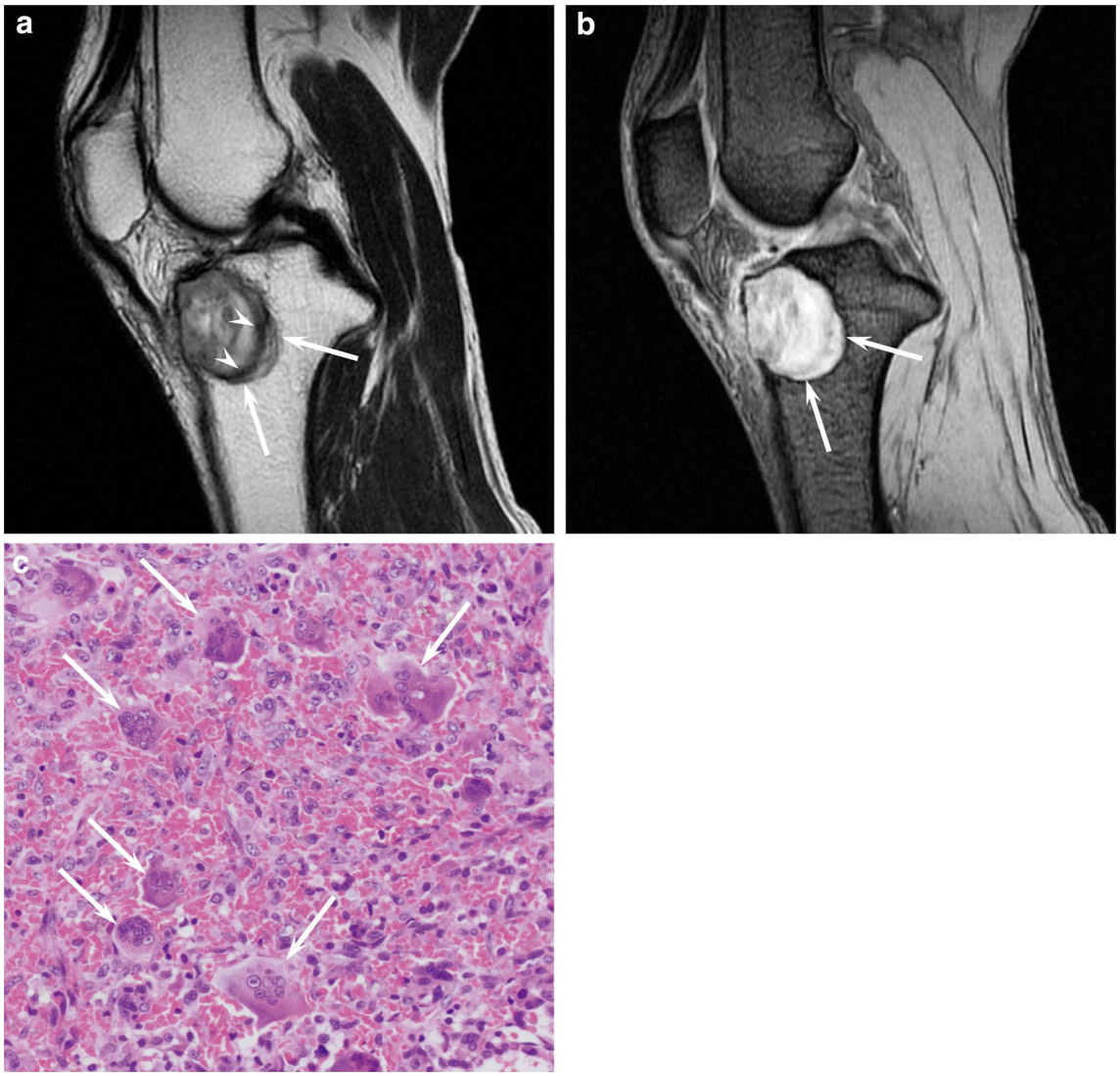

Fig. 3 A 60-year-old man with GCT of left distal femur (case 10). **a** T2-weighted fast spin-echo (TR/TE 4,000/100 ms) sagittal image shows a heterogeneously hyperintense lesion (arrows) with hypointense areas (arrow heads). **b** T2*-weighted gradient-echo (TR/TE 550/10 ms) sagittal image shows heterogeneous hyperintensity within the tumor (arrows). **c** Open biopsy specimen (H&E stain, 200× magnification) shows multinucleated giant cells without hemosiderin deposition (arrows) among numerous extravasated erythrocytes. This case was judged as a small amount of hemosiderin deposition and a large amount of hemorrhage

and the tumor becomes covered by a thin shell of subperiosteal new bone, causing expansion of the contour of bone [12]. GCTs may demonstrate aggressive features, such as cortical destruction and associated soft-tissue mass [2]. The tumor tissue comprising GCTs is often soft, friable, and fleshy, with a variable appearance, which includes areas of fibrosis, necrosis, hemorrhage, hemosiderin deposition, cystic formation, and xanthomatous histiocytes [3, 5]. The vascular stroma of GCTs usually contains numerous thin-walled vascular channels, predisposing areas to hemorrhaging [10, 13]. Areas of necrosis and hemorrhage are often responsible for a prominent cystic appearance. Cystic GCTs may mimic aneurysmal bone cysts; however, they contain additional solid areas with typical histological features of GCTs.

Hemosiderin deposition is a characteristic pathological feature of GCT and is associated with excessive amounts of iron, usually caused by phagocytosed extravasated erythrocytes [11, 13]. Aoki J et al. reported that a large amount of hemosiderin was pathologically confirmed in 10 of 16 (61%) GCTs with hypointensity on MR images, whereas the remaining 6 of 16 (39%) GCTs without hypointensity on MR images revealed little-to-no hemosiderin deposition [11]. This suggests that the amount of hemosiderin is strongly associated with hypointensity on MR images. Although hypointensive areas within GCTs were demonstrated on

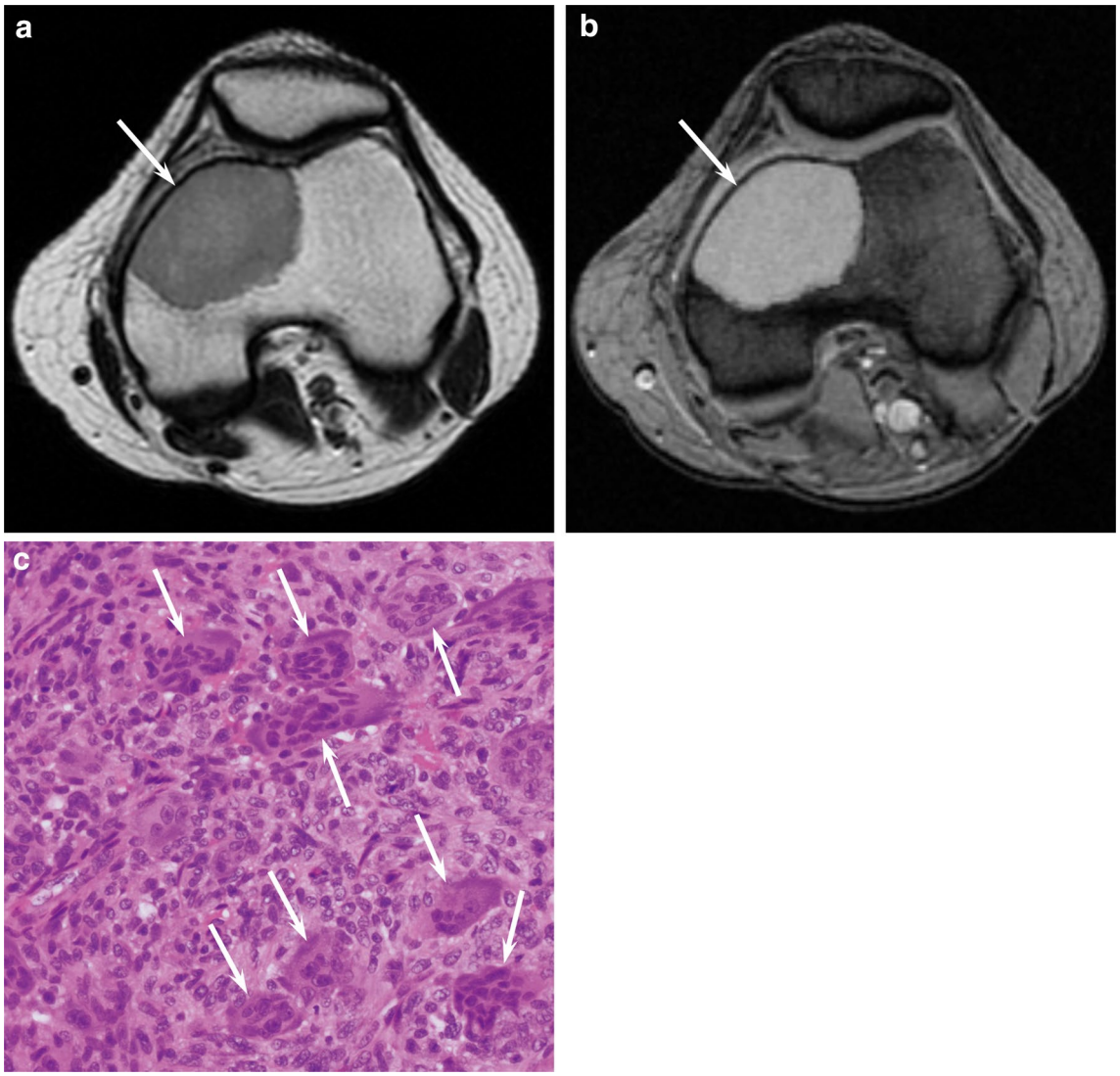

Fig. 4 A 40-year-old man with GCT of left distal femur (case 11). **a** T2-weighted fast spin-echo (TR/TE 4,200/100 ms) image shows a homogeneously mild hyperintense lesion (arrow) without hypointense areas. **b** T2*-weighted gradient-echo (TR/TE 584/11 ms) image shows homogeneous hyperintensity within the tumor (arrows). **c** Open biopsy specimen (H&E stain, 200× magnification) shows multinucleated giant cells without hemosiderin deposition (arrows). This case was judged as a small amount of hemosiderin deposition and hemorrhage

T2*-weighted images in one case in this paper [11], to our knowledge, no previous studies have assessed the detailed T2*-weighted imaging findings of GCTs.

In the present study, T2* hypointensity was observed in 6 of 12 (50%) GCTs. Among the six GCTs with T2* hypointensity, a large amount of hemosiderin deposition was pathologically observed in five (83%) cases, whereas a small amount of hemosiderin deposition was observed in one (17%) case. Conversely, among the six GCTs without T2* hypointensity, a small amount of hemosiderin deposition was pathologically observed in all six (100%). Although T2* hypointensity within the tumor was clearly demonstrated in case number 6, a small amount of hemosiderin deposition was revealed by open biopsy specimen (Figs. 2). Possible reasons for the discrepancy between radiological and pathological findings using post-biopsy MR images were explored and it was found that open biopsy sites assessed by an orthopedic surgeon contained fewer hemorrhagic areas, suggesting that T2* hypointensity within GCT corresponded with hemosiderin deposition.

In the present study, T2* hypointensity was observed in 10 of 12 (83%) GCTs. Among the 10 GCTs with T2 hypointensity, a large amount of hemorrhage was pathologically observed in 9 (90%) cases, whereas a small amount of hemorrhage was observed in one (10%) case. Conversely, among the two GCTs without T2 hypointensity, a small amount of

hemorrhage was pathologically observed in all two (100%). As mentioned above, the discrepancy between radiological and pathological findings was also observed in case number 6. Although collagenous fibrous tissue, granulomatous tissue, and calcification are also possible causes of T2 hypointensity, it is suggested that T2 hypointensity within GCT corresponded with hemorrhaging.

In this study, septal formation and cystic formation on T2-weighted images were significantly more frequent in GCTs with T2* hypointensity compared to those without. Cystic formation is usually caused by necrosis and hemorrhage; thus, it is reasonable to conclude that GCTs with hemosiderin deposition tend to have a cystic appearance. Septal formation is considered to be similar in structure to cyst walls; thus, both septal formation and cystic formation are associated with intratumoral hemorrhaging.

This study has several limitations that should be noted. First, the study was conducted at a single institution with a small sample population. Although 33 patients with histopathologically proven GCT were confirmed, 1.5-T MR imaging, including T2*-weighted imaging, was performed in only 12 patients. This is because T2*-weighted imaging did not usually include a routine protocol for bone tumors, and T2*-weighted imaging was performed only in patients with suspected GCT before MR examinations. Second, pathological assessment was performed using open biopsy specimens. Majority of the 12 patients were treated by curettage, making an accurate radiological–pathological correlation difficult to achieve using these specimens. In addition, we avoided using curettage specimens for the pathological evaluation in this study, because of the fact that open biopsy may cause hemorrhaging in curettage specimens. Third, owing to the retrospective nature of this study, two different MR scanners were used; however, the results would not be considerably different if images were obtained using the same MR scanner, as only conventional MR sequences were assessed in this study.

In conclusion, half of the GCTs showed T2* hypointensity, suggestive of hemosiderin deposition, whereas the other half of GCTs did not show T2* hypointensity, due to a small amount of hemosiderin deposition. In addition, a large amount of hemorrhage was pathologically observed in 90% of GCTs with T2 hypointensity. Conversely, a small amount of hemorrhage was pathologically observed in all cases of GCTs without T2 hypointensity. Consequently, GCTs rarely showed non-specific hyperintensity without hypointense areas on T2*- and T2-weighted images, reflecting a small amount of hemosiderin deposition and hemorrhage.

Funding The authors declare that there is no funding.

Compliance with ethical standards

Conflict of interest The authors declare that they have no conflict of interest.

Ethical statement The authors declare that they preserve ethical standards.

References

1. Sobti A, Agrawal P, Agarwala S, Agarwal M. Giant cell tumor of bone—an overview. Arch Bone Jt Surg. 2016;4(1):2–9.
2. Chakarun CJ, Forrester DM, Gottsegen CJ, Patel DB, White EA, Matcuk GR Jr. Giant cell tumor of bone: review, mimics, and new developments in treatment. Radiographics. 2013;33(1):197–211.
3. Murphey MD, Nomikos GC, Flemming DJ, Gannon FH, Temple HT, Kransdorf MJ. Imaging of giant cell tumor and giant cell reparative granuloma of bone: radiologic-pathologic correlation. Radiographics. 2001;21(5):1283–309.
4. Stacy GS, Peabody TD, Dixon LB. Mimics on radiography of giant cell tumor of bone. AJR Am J Roentgenol. 2003;181(6):1583–9.
5. Mavrogenis AF, Igoumenou VG, Megaloikonomos PD, Panagopoulos GN, Papagelopoulos PJ, Soucacos PN. Giant cell tumor of bone revisited. SICOT J. 2017;3:54.
6. Bridge JA, Neff JR, Mouron BJ. Giant cell tumor of bone: chromosomal analysis of 48 specimens and review of the literature. Cancer Genet Cytogenet. 1992;58(1):2–13.
7. Fazekas F, Kleinert R, Roob G, Kleinert G, Kapeller P, Schmidt R, et al. Histopathologic analysis of foci of signal loss on gradient-echo T2*-weighted MR images in patients with spontaneous intracerebral hemorrhage: evidence of microangiopathy-related microbleeds. AJNR Am J Neuroradiol. 1999;20(4):637–42.
8. Tsushima Y, Aoki J, Endo K. Brain microhemorrhages detected on T2*-weighted gradient-echo MR images. AJNR Am J Neuroradiol. 2003;24(1):88–96.
9. Shams S, Martola J, Cavallin L, Granberg T, Shams M, Aspelin P, et al. SWI or T2*: which MRI sequence to use in the detection of cerebral microbleeds? The Karolinska Imaging Dementia Study. AJNR Am J Neuroradiol. 2015;36(6):1089–95.
10. Aoki J, Moriya K, Yamashita K, Fujioka F, Ishii K, Karakida O, et al. Giant cell tumors of bone containing large amounts of hemosiderin: MR-pathologic correlation. J Comput Assist Tomogr. 1991;15(6):1024–7.
11. Aoki J, Tanikawa H, Ishii K, Seo GS, Karakida O, Sone S, et al. MR findings indicative of hemosiderin in giant-cell tumor of bone: frequency, cause, and diagnostic significance. AJR Am J Roentgenol. 1996;166(1):145–8.
12. Purohit S, Pardiwala DN. Imaging of giant cell tumor of bone. Indian J Orthop. 2007;41(2):91–6.
13. Lee MJ, Sallomi DF, Munk PL, Janzen DL, Connell DG, O'Connell JX, et al. Pictorial review: giant cell tumours of bone. Clin Radiol. 1998;53(7):481–9.